Cell Reports, Volume *24*

Supplemental Information

Aberrant Calcium Signaling in Astrocytes Inhibits Neuronal Excitability in a Human Down Syndrome Stem Cell Model

Grace O. Mizuno, Yinxue Wang, Guilai Shi, Yizhi Wang, Junqing Sun, Stelios Papadopoulos, Gerard J. Broussard, Elizabeth K. Unger, Wenbin Deng, Jason Weick, Anita Bhattacharyya, Chao-Yin Chen, Guoqiang Yu, Loren L. Looger, and Lin Tian

Supplementary Information

1. Supplementary Figures

A

Cell line identifier	Karyotype	Source fibroblasts	Reprogramming method
DS2U	Euploid	AG05397, male, 1 year	Retrovirus
DS1	Ts21	AG05397	Retrovirus
DS4	Ts21	AG05397	Retrovirus

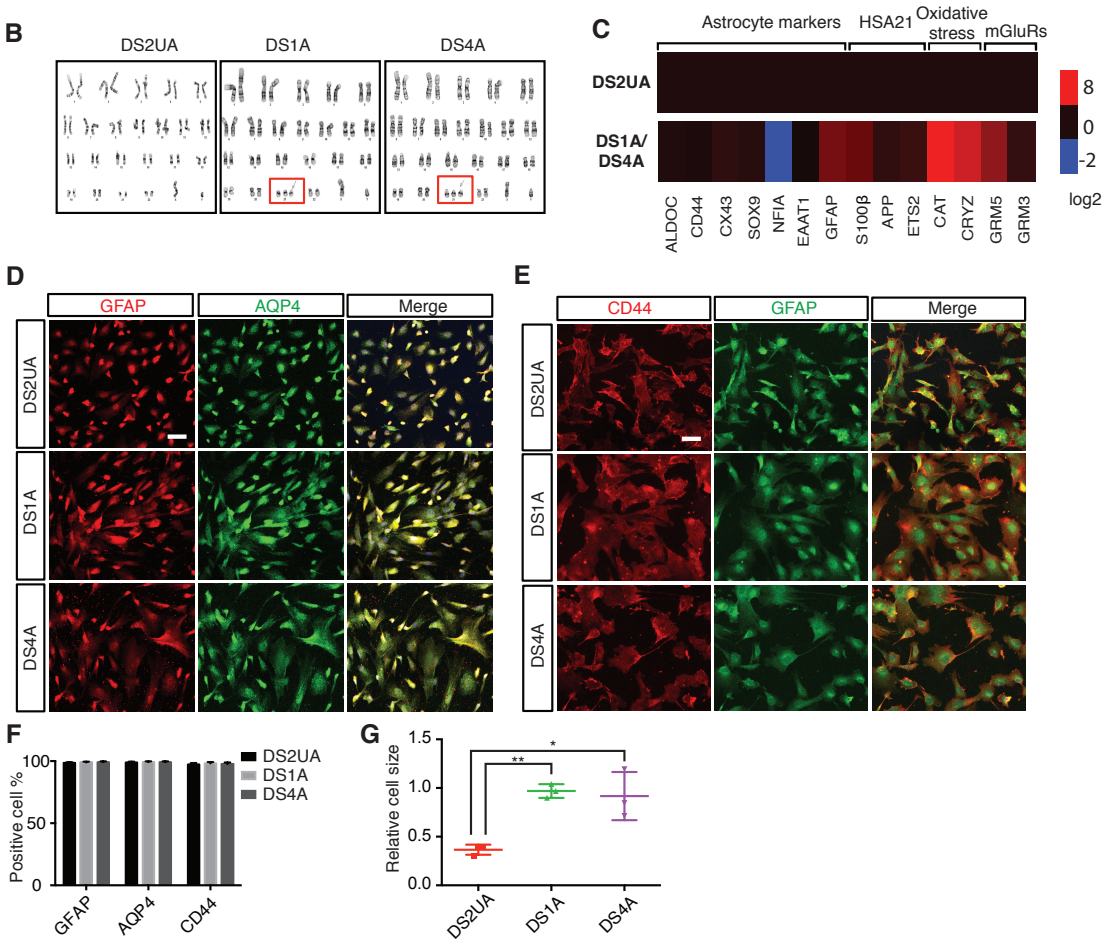

Figure S1. Differentiation and characterization of human iPSC-derived astroglia. Related to Figure 1. (a) Table of differentiated lines used in this study. (b) Karyotype analysis of human iPSC-derived astroglia and primary astrocytes (HA). Trisomy of HSA21 indicated with red boxes. (c) qPCR analysis of astrocytic markers, genes on HSA21, or genes associated with oxidative stress in iPSC-derived astroglia. The expression levels of genes in DS astroglia (DS1A and DS4A) were normalized to levels in isogenic DS2UA. (d-f) Astrocyte markers, such as GFAP, AQP4 and CD44, were broadly expressed in human iPSC-derived astroglia. Co-immunostaining of GFAP with AQP4 (d) or CD44 (e) and quantitation (f) are shown. Scale bar: 50 μm. (g) Relative cell sizes of iPSC-derived astroglia.

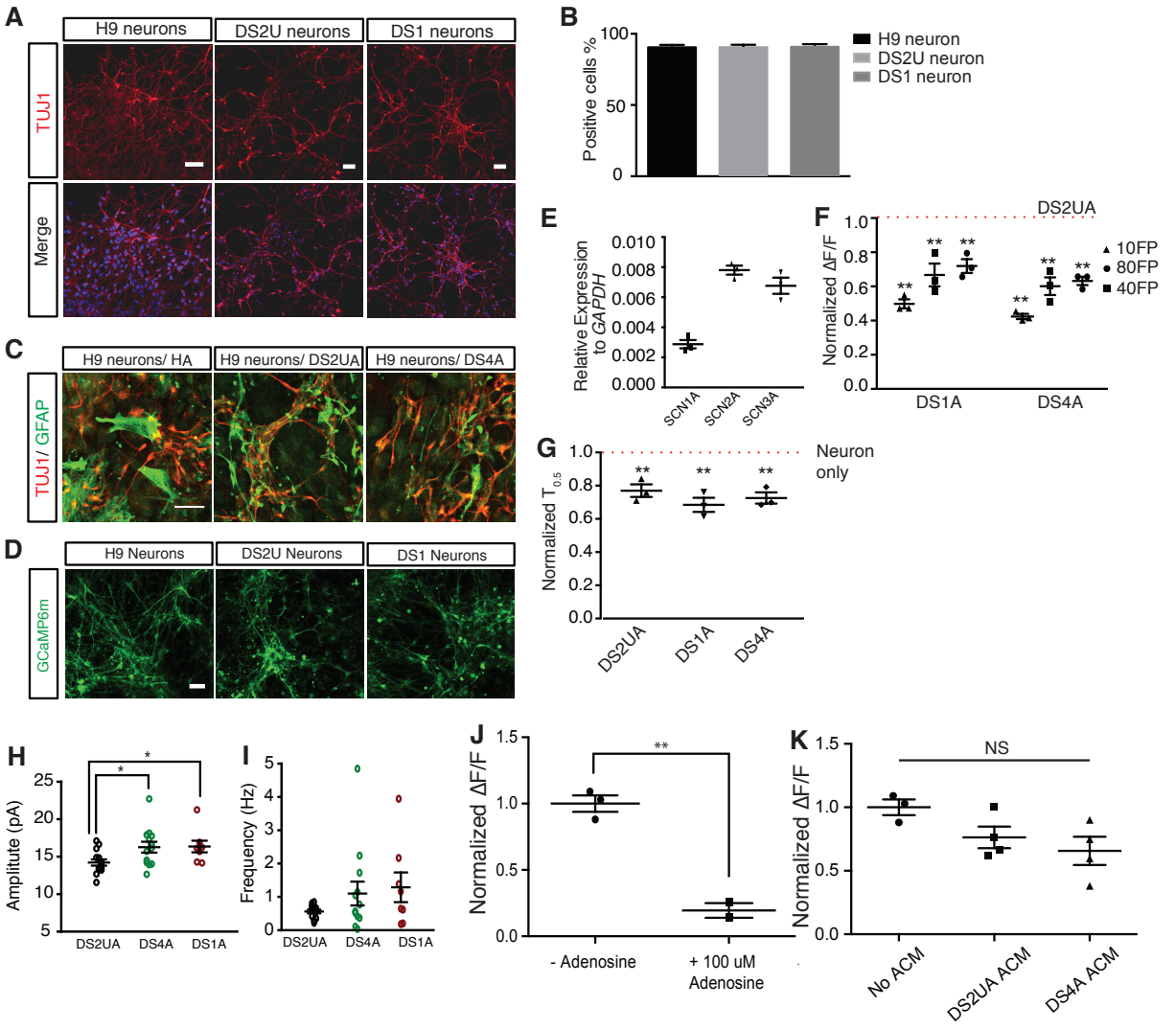

Figure S2. Characterization of ESC or iPSC-derived neurons. Related to Figure 1. (a) Expression of TUJ1 in H9 hESC, isogenic DS2U and DS1 iPSC-derived neurons. (b) Percentage of neurons showing expression of TUJ1. (*n*=3 images of immunostaining) (c) Expression of TUJ1 and GFAP in H9-neurons co-cultured with control HA, isogenic control DS2UA and DS1A. (d) Expression of GCaMP6m in H9 hESC, isogenic DS2UA and DS1 iPSC-derived neurons. (e) Real-time qPCR analysis of the expression of voltage gated sodium channels in H9 hESC-derived neurons, normalized to GAPDH (*n*=3). (f) ΔF/F of H9 hESC-derived neurons in response to a variety of FPs when co-cultured with DS1A or DS4A. ΔF/F was normalized to that when co-cultured with DS2UA (red dotted line). (g) Response kinetics of H9 hESC-derived neurons to 40 FPs, when co-cultured with DS2UA, DS1A or DS4A normalized to that of neurons alone (red dotted line) (*n*=3) (h) The mean amplitude was significantly higher in DS4A and DS1A compared to the DS2UA group (Fisher's LSD test, $p<0.05$). (i) Although there was a trend for higher mEPSC frequencies in the DS4A and DS1A groups, the differences were not statistical significant. (j-k) Suppressed neuronal activity is influenced by purinergic signaling. (j) H9-neurons incubated with 100 µm adenosine resulted in suppressed neuronal activity (normalized ΔF/F of 100 µM adenosine (*n*=2) to without adenosine (*n*=3) =0.20±0.06, *P*=0.0032). (k) H9-neurons incubated with DS4A or DS4A ACM trended towards suppressed neuronal activity (ACM from DS4A suppressed neuronal excitability by 0.34-fold versus 0.24-fold from DS2UA ACM normalized to no ACM (*n*=3), *P*=0.06 DS4A (*n*=4), *P*=0.091 DS2UA (*n*=4)).

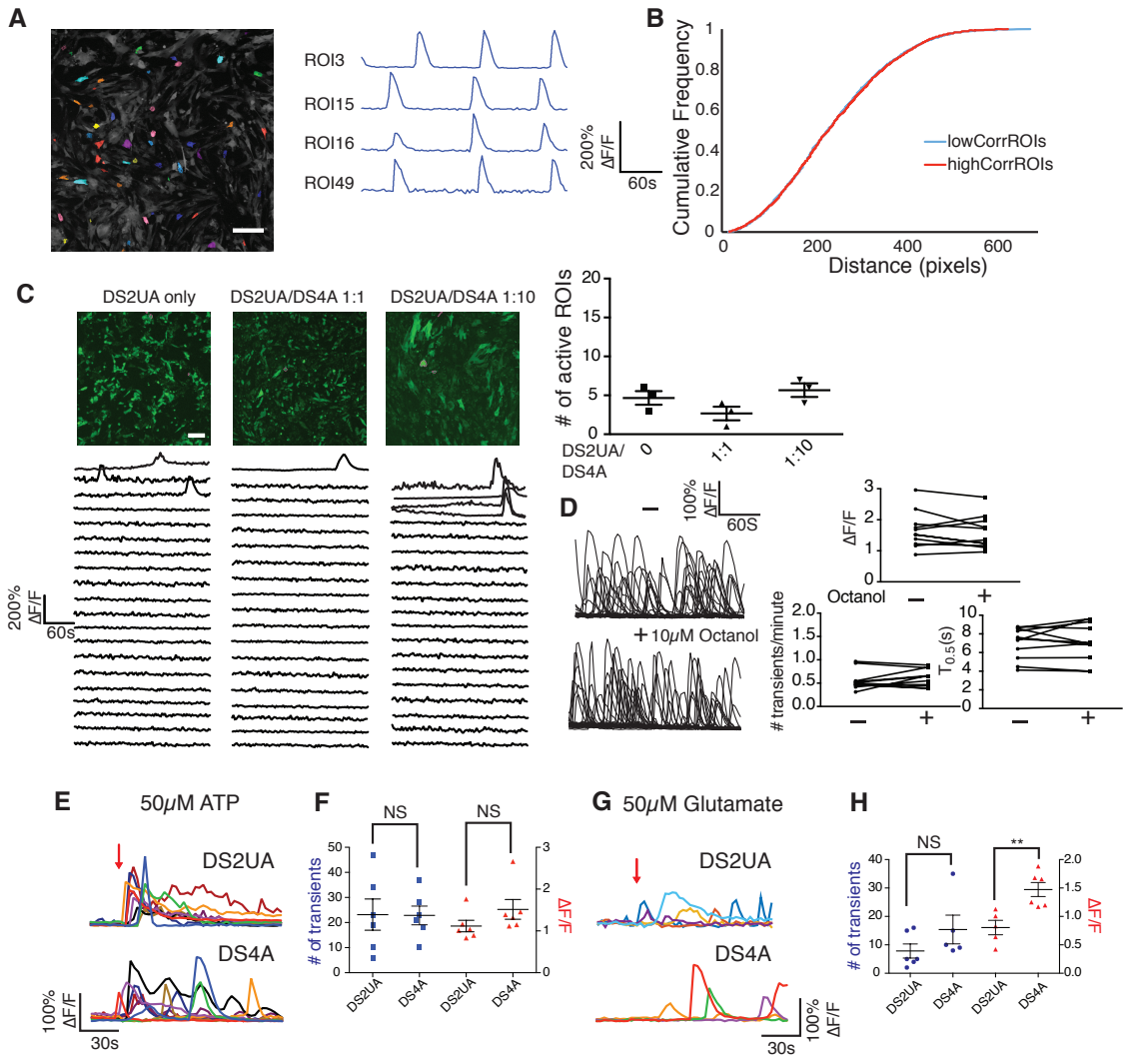

Figure S3. Fluctuation dynamics and Ca^{2+} fluctuations in isogenic and DS astroglia. Related to Figure 2. (a-d) Spontaneous calcium could not be induced in isogenic astroglia when co-cultured with DS astroglia. (a-b) Analysis of Ca^{2+} transients revealed 33 clusters of cells (n=93) in DS4A with correlated temporal dynamics (a), while their locations were randomly distributed (b). Each cluster was labeled with a specific color, and Ca^{2+} traces from one representative cluster in 5 min is shown. Scale bar: 200 μm (a). Temporally correlated ROIs showed similar spatial distribution with randomly selected ROIs that were not correlated in temporal dynamics. (c) The number of active ROIs (3 imaging sessions of 5 min) in DS2UA alone or in the presence of co-cultured DS4A at different ratios. Ca^{2+} traces from 20 ROIs are also shown. (d) The gap junction blocker octanol failed to modulate the properties of spontaneous Ca^{2+} fluctuations in DS4A. Representative traces of Ca^{2+} fluctuations (n=11) without treatment and in the presence of 10μM octanol. Quantification of the amplitude, frequency and $T_{0.5}$ of these Ca^{2+} fluctuations before and after treatment. Scale bar: 100 μm. (e-h) Astroglia response to ATP and glutamate. Representative Ca^{2+} responses of control isogenic DS2UA and DS4A were shown in selected region of interests (10 ROIs for ATP (e) and 5 ROIs for glutamate (g)). Number of Ca^{2+} transients in 150 s with addition of 50 μM ATP and their averaged ΔF/F (f) from at least 3 independent imaging sessions. Number of Ca^{2+} transients in 150 s, with addition of 50 μM glutamate and their averaged ΔF/F (h).

A

Gene group	Genes
mGluRs	GRM1/2/3/4/5/6/7/8
Purinergic receptors	P2RY1, ADORA1, ADORA2A, ADORA2B, ADORA3
GPCR pathway	GNAQ, SHANK1/2/3
ER Ca^{2+}	$IP_3R1/2/3$, RYR1/2/3, ATP2A1
Mitochondrial Ca^{2+}	NCLX, MCU
Plasma membrane Ca^{2+}	STIM1, ORAI1/2/3, NCX1/2/3, ATP2B1, TRPA1
Astroglial markers	S100β, SOX9, FABP7, NF1A, EAAT1/2, CX43, AQP4, ALDOC, CD44

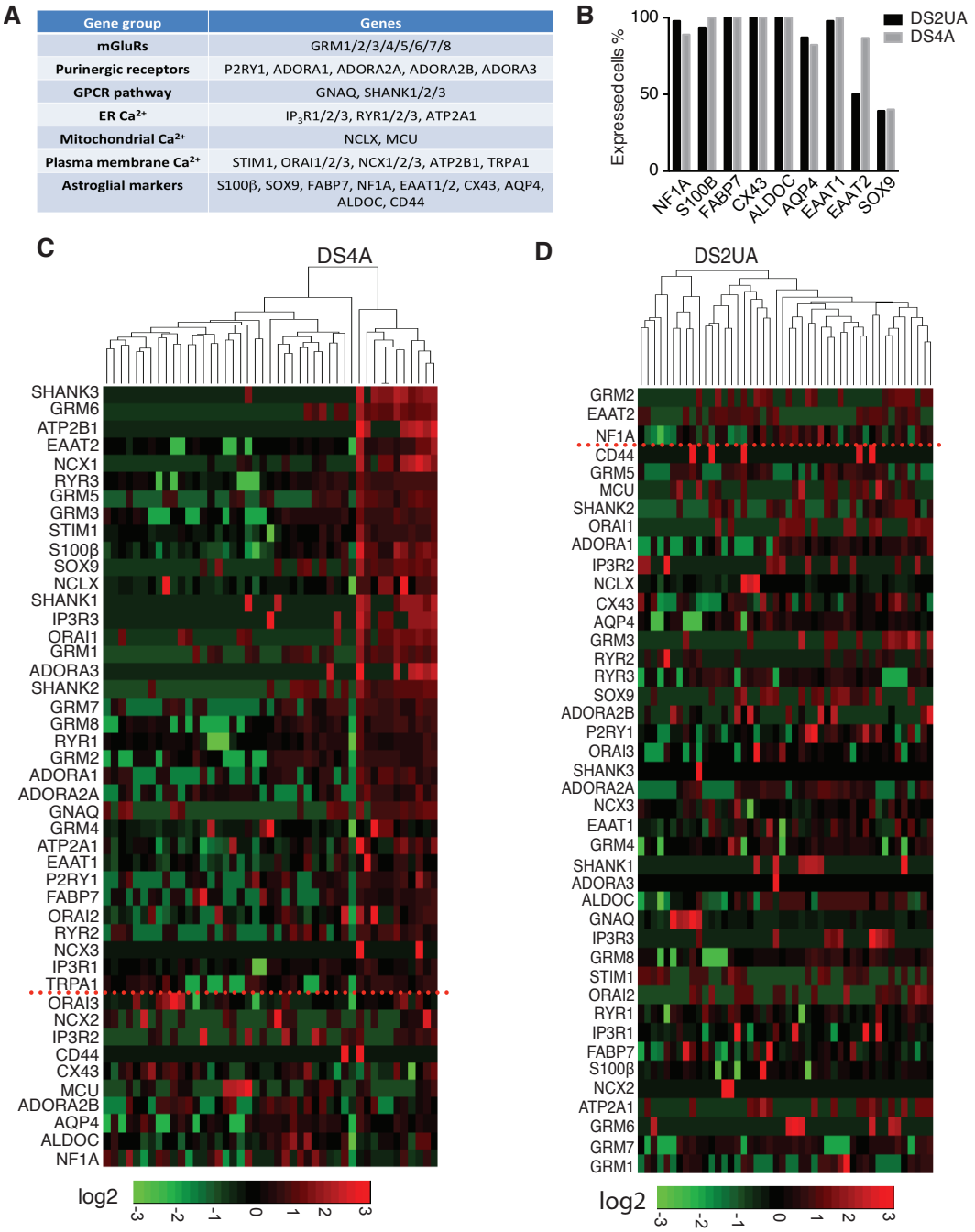

Figure S4. Single-cell gene expression analysis of human iPSC-derived astroglia. Related to Figure 4 and Figure 5. (a) Table of selectively analyzed gene transcripts encoding Ca^{2+} handling toolkits as well as cell-type specific markers. (b) Percentage of cells expressing a given cell-specific markers (n=46 for DS2UA and 45 for DS4A). (c-d) Heatmaps showing the expression of gene transcripts encoding astroglial markers and Ca^{2+} handing toolkits, including mGluRs, purinergic receptors and intracellular Ca^{2+} pathways, in individual cells of DS4A (c) and DS2UA (d). Each row represents a single astroglia. Dendrograms show unsupervised clustering based on differentially expressed genes. Genes are listed from top to bottom showing greatest to least differences between the two clusters (unsupervised clustering analysis). Red line shows threshold of $P<(0.05)$.

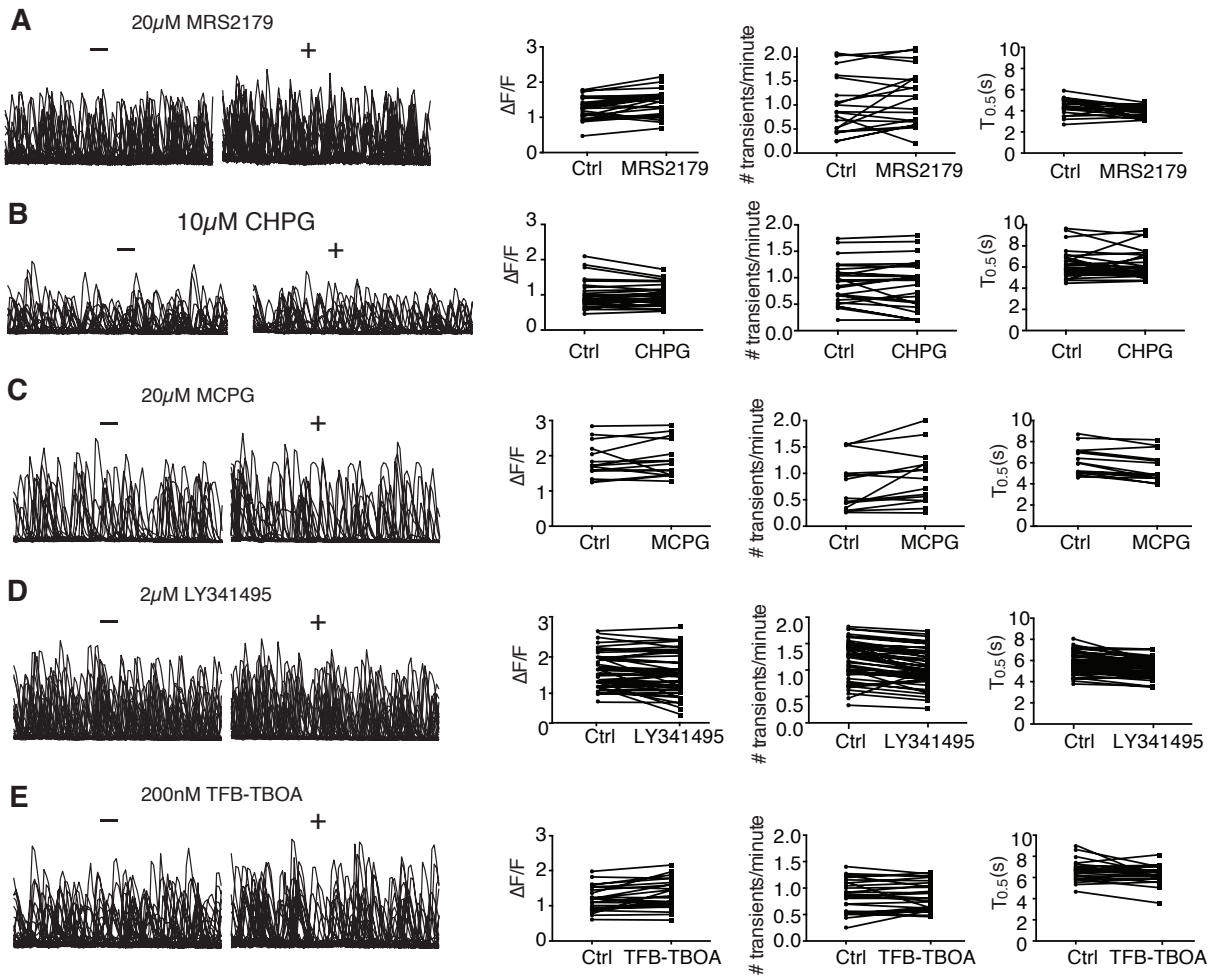

Figure S5. The effect of antagonists on Ca^{2+} fluctuations in DS4A. Related to Figure 4. Representative traces of Ca^{2+} fluctuations in the absence and presence of antagonists including mGluR5 agonist CHPG (30 ROIs, a) MRS2179 (24 ROIs, b), MCPG (15 ROIs, c), LY341495 (53 ROIs, d), and TFB-TBOA (28 ROIs, e). The amplitude, frequency and $T_{0.5}$ of these Ca2+ fluctuations before and after treatment are also shown.

2. Table S1. Gene and protein abbreviations

ALDOC	Aldolase, fructose-bisphosphate C
APP	Amyloid beta precursor protein
AQP4	Aquaporin 4
ATP2B1	ATPase plasma membrane Ca^{2+} transporting 1
CAT	Catalase
CD44	CD44 cell adhesion molecule
CRYZ	Crystallin zeta
CX43	Connexin 43
DSCAM	Down syndrome cell adhesion molecule
DYRK1A	Dual specificity tyrosine phosphorylation regulated
EAAT1	Excitatory amino acid transporter 1
EAAT2	Excitatory amino acid transporter 2
ETS2	ETS proto-oncogene 2, transcription factor
GFAP	Glial fibrillary acidic protein
IP3R3	Inositol 1, 4, 5-triphosphate receptor type 3
KCNJ6	Potassium voltage-gated channel subfamily J member 6
mGluRs	Metabotropic glutamate receptors (GRM3, GRM5)
miR-155	MicroRNA 155
NCLX	Sodium/ potassium/ calcium exchanger
NCX1	Sodium/ calcium exchanger
NF1A	Nuclear factor I A
NKCC1	Sodium potassium chloride transporter
ORAI	Calcium release activated calcium channel protein
P2R	Purinergic receptors
RYR1/3	Ryanodine receptor
S100β	S-100 calcium-binding protein subunit β
SIM2	Single-minded transcription factor 2
SOX9	Protein critical for embryonic development
STIM	Stromal interaction molecules

3. Supplementary Materials and Methods

Lentivirus production

Lentiviruses were produced by co-transfecting HEK293T cells (ATCC) with 5 μg pSIV-*Synapsin-1*-GCaMP6m or pHIV-*EF1α*-Lck-GCaMP6m, scrambled or S100β shRNAs, 2 μg pHCMV-G, and 3 μg pCMV-deltaR8.2, using 40 μl SuperFect (Qiagen, 301305). Supernatant containing viral particles was collected, filtered, and concentrated 72 h later with an Ultra-4 centrifugal filter (Millipore, UFC810024).

mEPSC recordings and analysis

Whole-cell voltage clamp experiments were performed 17–19 days after plating. mEPSCs were recorded in an external solution containing 140 mM NaCl, 5 mM KCl, 10 mM HEPES, 2 mM CaCl2, 1 mM MgSO4, 1 μM tetrodotoxin (TTX), 50 μM AP-5, and 20 μM bicuculline (pH 7.4 with NaOH, 290 mOsm/l). Borosilicate glass electrodes were filled with an internal solution containing 145 mM CsCl, 1 mM EGTA, 5 mM HEPES, 0.1 mM CaCl2, 2 mM MgSO4 (PH 7.4 with CsOH, 275 mOsm/l). The seal resistance was greater than 1 GΩ and the series resistance was no greater than 20 MΩ. All recordings were made with an Axopatch 200B patch-clamp amplifier (Axon Instruments, Foster City, CA, USA). Whole-cell currents were filtered at 2 kHz and digitized at 10 kHz. All neurons were voltage-clamped at –60 mV. The mEPSC events were detected with Mini Analysis software (Synaptosoft Inc., Fort Lee, NJ, USA). The accuracy of detection was confirmed by visual inspection.

Immuncytochemistry

Cells maintained on cover glasses (Fisher Scientific, 12-545-81) were washed with PBS 3 times before being fixed with 4% paraformaldehyde (VWR, 100503-916) for 15 min. After washing, cells were treated with 0.1% Triton X-100 (Fisher Scientific, BP151-500) for 10 min, blocked

with 10% bovine serum albumin (Sigma, A9647) for 60 min, and incubated with primary antibodies at 4 °C overnight followed by secondary antibodies for 1 h at room temperature. Cells were washed with PBS 2 times after each antibody incubation and mounted on glass slides (Fisher Scientific, 12-550-123) using ProLong® Gold Anti-fade Mountant with DAPI (Thermo Fisher Scientific, P36935). Primary antibodies used included: AQP4 (Santa Cruz Biotech, sc-20812, rabbit), CD44 (Abcam, ab6124, mouse), GFAP (Millipore, MAB360, mouse; AB5840, rabbit), TUJ1 (COVANCE, MMS-435P, mouse), Synapsin-I (Millipore, AB1543, rabbit), S100 β (Abcam, ab11178, mouse), and PSD95 (NeuroMab, K28/43, mouse). Secondary antibodies included Alexa488-conjugated donkey anti-rabbit (A21206) and Alexa594-conjugated goat anti-mouse (A11005), and were purchased from Thermo Fisher Scientific.

Immunocytochemistry analysis

Images were obtained using a Zeiss LSM 710 confocal microscope (× 40 magnification, N.A. 1.3 oil objective). All immunostaining experiments were performed 3 times, and representative results were presented.

Puncta density quantification: Using the spot-detection feature in the Imaris software (Bitplane) the number of colocalized Synapsin-1 and PSD95 per μm of dendrite was obtained to calculate the puncta density. S100 β immunocytochemistry analysis: Using FIJI the fluorescence intensity of each imaging field was analyzed.

Ca^{2+} imaging analysis of astrocytes using FASP

As an unsupervised analytic method, FASP is data-driven, learning model parameters using machine-learning techniques to automatically detect ROIs displaying Ca^{2+} fluctuation. In addition, designed under probabilistic principles, FASP has strong statistical power to detect

weak signals (ROIs) that are easily ignored by purely manual analysis. Our simulation study verified that some ROIs with weak signals were ignored by manual analysis but correctly detected by FASP. By judicious application of various statistical theories, FASP confers tuning parameters with probabilistic meaning, which can be directly translated into the false discovery rates. This algorithm greatly facilitates the usability of parameter settings and ensures the reproducibility of the results and equal comparison across experiments.

Specifically, we set a single threshold corresponding to a false discovery rate of 0.01; that is, an average of 1% of all identified active ROIs are expected to be false positives. The threshold is fixed for all experiments and conditions.

Given a time-lapse astrocytic Ca^{2+}-imaging data set, FASP generates a set of ROIs and corresponding characteristic curves. For each pixel in an ROI, there is a corresponding activity curve for which the time shift with respect to the characteristic curve is also estimated. Based on the results of FASP, we quantified various parameters of astrocytic Ca^{2+} signals according to the following:

- The signal-to-baseline ratio of fluorescence was calculated as

$$\frac{\Delta F}{F_0} = \frac{F - F_0}{F_0},$$

  where the baseline fluorescence F_0 is estimated as the 10^{th} percentile of the fluorescence level over all time points of the measurement.
- The number of Ca^{2+} transients is calculated as the number of peak responses from all ROIs detected in each time-lapse imaging session.
- The number of active ROIs is calculated as the total number of ROIs detected by FASP in the field of view of each time-lapse imaging session.

Amplitude: To calculate the amplitude of a Ca^{2+} transient we first transformed the raw time-intensity curves into signal-to-baseline ratio of fluorescence ($\Delta F/F0=(F-F0)/F0$), where the baseline fluorescence F0 is estimated as the 10^{th} percentile of the fluorescence levels (intensities) at all the time points during measurement.

Frequency: To calculate the frequency of Ca^{2+} fluctuations more reliably, we first determined the average duration between 2 contiguous events, and then defined the frequency as the inverse of the average duration. For those ROIs that only displayed single Ca^{2+} transients during the imaging session, the information contained in the single-event time series is insufficient for point estimation of frequency. These ROIs are expected to have a positive frequency between 0 and 0.2 transients per minute.

$T_{0.5}$: Decay kinetics or $T_{0.5}$(off) was calculated using linear interpolation as the time from peak to half-amplitude of an event.

Propagation speed wavefront analysis: On the basis of estimated pixel-wise time shifts from the characteristic curve, wavefronts of Ca^{2+} transients were located; accordingly, the propagation speed of Ca^{2+} events within an ROI was obtained by estimating the average distance between wavefronts. Active ROIs detected in DS4A were divided into 33 clusters of timed coincidence by unsupervised clustering analysis (Affinity Propagation Clustering Algorithm)[57]. Any pairs of ROIs within the same cluster were recognized as highly coincident, while any pairs of ROIs from 2 different clusters were recognized as weakly coincident. Distributions of pixel distance of correlated and uncorrelated pairs were then measured and plotted.

Neuron-astrocyte co-culture or astrocyte conditioned media imaging

All neuronal imaging experiments were repeated 3 times, and 10 ROIs were selected for analysis using a customized script (FluoAnalyzer) in MATLAB (MathWorks). ROIs (*n*>10 for each imaging file) were manually selected, and the fluorescence intensity (F) at each frame was quantified as the mean of all selected ROIs. The neuronal responses were calculated as ΔF/F ($F-F_0/F_0$), where F was quantified as the mean of all selected ROIs (*n*>10 in each field of view), and F_0 was taken as the mean of all ROIs across the first 3 frames.

RNA isolation and qPCR

Total RNA was prepared from cells *(n*=3) with RNeasy kit (Qiagen, 74104). Complementary DNA was prepared with iScript RT Supermix (Bio-Rad, 170-8841). qPCR was performed with iTaq™ Universal SYBR® Green Supermix (Bio-Rad, 172-5121) on a CFX96™ Real-Time System (Bio-Rad), and the data was collected with Bio-Rad CFX Manager 3.0. Gene expression levels were quantified relative to the housekeeping gene, *GAPDH*.

Single-cell expression analysis

The values of gene expression were pre-processed by taking the inverse, applying a square-root transformation, and rescaling the expression to zero mean and unit variance. The similarity matrix was computed first using the default method of negative distance (default parameters), and affinity propagation clustering was applied by setting the desired number of clusters to 2 in the R package, Apcluster.

The single-cell expression analysis consisted of 4 major components as detailed below:

Preprocessing: In the raw data, the value for each gene denotes how many amplification

cycles were required to cross the threshold, which is set using the AutoGlobal method. In our data, the maximum observed value was 29. A missing value indicated that the corresponding gene had too little expression to be amplified to reach the threshold quantity. In the raw data, missing values were marked by 999. We replaced all missing values by 60, which was around 2 times the maximum value observed. Then, the inverse of the values was used to represent the amount of expression. A square-root transformation was applied to each gene to normalize for expression-level differences. Finally, for each cell, all genes were normalized to have zero mean and unit variance to highlight differences between cells.

Clustering analysis: Affinity propagation clustering (APC) was applied. The algorithm was implemented in the R package, Apcluster. The algorithm requires users to input a similarity matrix. The default settings were adopted; in other words, Euclidian distance was calculated based on the data matrix and the negative distance was used as the similarity matrix. To be consistent with the observation that there were 2 groups of astrocytes, one with active Ca^{2+} fluctuations and the other one without, the desired number of clusters was set to 2. Notably, we did not know which cells were active, and the analysis was unsupervised.

Assessing statistical significance of resultant clusters: Since a clustering algorithm can always generate clusters even if there are no clusters actually present in the data, we sought to evaluate whether the resultant clusters were purely by chance. The null hypothesis was that there were no groups of cells that were closer within-group than between-groups (i.e., distances between cells were uniformly distributed). Permutation was used to generate the distribution for the null hypothesis. All genes in the data set were permuted 100,000 times, resulting in 100,000 data sets following the null hypothesis. For each resulting data set, we ran APC to get 2 groups. In APC, the objective function was the overall similarity. A histogram was obtained based on the

100,000 overall similarities. The position of the observed overall similarity indicated the significance of the observed value.

Differentially expressed genes between clusters: Standard differential analysis, such as t-test between groups, cannot be applied here because the clustering was based on all genes; hence, each gene was biased toward differential expression between clusters. To correct for this bias, a permutation procedure was designed. To test the significance for each gene, we shuffled the values in that gene 10,000 times while keeping all other genes fixed. In this way, the gene would not interfere with the clustering results, so there would be no bias. Each time we ran the clustering algorithm APC to get 2 groups. Based on the new clustering results, the significance of the gene was recorded and summarized into a histogram, which could be further used to derive the corrected *P* value. For example, if the original *P* value was 0.01, corresponding to the 2^{nd} percentile in the histogram, the corrected *P* value would be 0.02.

Fluorescence-activated cell sorting (FACS)

DS astrocytes were infected with lentiviruses expressing S100β-shRNA-mCherry and collected 3 days later for sorting, which was performed by the FACS core at UC Davis. The top 15% of cells expressing high amounts of mCherry measured on fluorescence intensity were collected as mCherry “high”, and the bottom 18% of cells expressing low amounts of mCherry were collected as “low”. High mCherry fluorescence represents high expression of S100β shRNA and less expression of S100β.

Inhibiting extracellular S100β

S100β (Abcam, ab11178) and TUJ1 (COVANCE, MMS-435P) antibodies (diluted 1:1000) were used to pretreat DS astrocytes for 10 minutes before imaging.